Malaysian Journal of Analytical Sciences (MJAS)



Published by Malaysian Analytical Sciences Society

SYNTHESIS AND CHARACTERISATION OF COMPOSITE SILICA, POLY(METHYL METHACRYLATE) (PMMA) AND GOLD-SILVER (Au-Ag) ALLOY VIA CO-CRYSTALLISATION FOR LIGHT MANIPULATION APPLICATIONS

(Sintesis dan Pencirian Komposit Silika, Poli(metil metakrilat) (PMMA) dan Aloi Emas-Perak (Au-Ag) Melalui Penghabluran Bersama Untuk Aplikasi Manipulasi Cahaya)

Rozaitunmas Jamal¹, Rabiatul Addawiyah Azwa Tahrin¹, Mohd Sabri Mohd Ghazali², Sibu C. Padmanabhan^{3,4}, Chan Kiki¹, and Syara Kassim^{2*}

¹Faculty of Science and Marine Environment,
Universiti Malaysia Terengganu, 21030 Kuala Nerus, Terengganu, Malaysia

²Advanced Nano Materials (ANoMa) Research Group,
Faculty of Science and Marine Environment,
Universiti Malaysia Terengganu, 21030 Kuala Nerus, Terengganu, Malaysia

³Advanced Materials and BioEngineering Research (AMBER) Centre,
Trinity College Dublin, Dublin 2, Ireland

⁴School of Chemistry,
Trinity College Dublin, College Green, Dublin 2, Ireland

*Corresponding author: syara.kassim@umt.edu.my

Received: 28 June 2022; Accepted: 23 November 2022; Published: 22 February 2023

Abstract

Metallodielectric photonic crystal has emerged as a formidable asset in the realms of light trapping materials. Inverted silica, and alloy noble metal nanoparticles of gold-silver alloy(Au-Ag) exhibited promising light trapping capabilities that have the potential of applications across many fields including solar cell, and biomedical device production. This composite was prepared via self-assembly; a fast, simple, and low-cost method capable of generating photonic crystals of greater surface area. Poly(methyl methacrylate) (PMMA) was used as the crystal template, and hydrolysed tetraethyl orthosilicate (TEOS) as the cementing component. In this study, methyl methacrylate monomer underwent a complete polymerisation reaction to form PMMA due to the absent of C=C bond around 1639.83 cm⁻¹ as characterised by IR spectroscopy. Alloy(Au-Ag) nanoparticles displayed good light absorption ability as shown from UV-Vis analysis of the nanoparticles at wavelength of 437nm. SEM imaging revealed that after the removal of PMMA template from Si-Alloy(Au-Ag)-PMMA composite, an inverted structure that possessed a hole skeleton structure was produced. The performance of the inverted Si-alloy(Au-Ag) composite was tested via a dye sensitive solar cell (DSSC) that showed an amplification in voltage reading.

Keywords: nanostructure, photonics, metallo-dielectric, alloy nanoparticles, inverse opal

Abstrak

Kristal fotonik metallodielektrik telah muncul sebagai aset yang menggerunkan dalam bidang bahan perangkap cahaya. Silika songsang, dan aloi nanopartikel logam adi daripada Aloi emas-perak (Au-Ag) mempamerkan keupayaan memerangkap cahaya yang mempunyai potensi aplikasi merentasi banyak bidang termasuk sel solar, dan pengeluaran peranti bioperubatan. Komposit ini disediakan melalui pemasangan sendiri; kaedah yang cepat, mudah dan kos rendah yang mampu menghasilkan kristal fotonik dengan luas permukaan yang lebih besar. Poli(metil metakrilat) (PMMA) digunakan sebagai templat kristal, dan tetraetil orthosilikat terhidrolisis (TEOS) sebagai komponen penyimenan. Dalam kajian ini, monomer metil metakrilat menjalani tindak balas pempolimeran lengkap untuk membentuk PMMA kerana ketiadaan ikatan C=C sekitar 1639.83 cm⁻¹ seperti yang dicirikan oleh spektroskopi IR. Nanozarah aloi (Au-Ag) menunjukkan keupayaan penyerapan cahaya yang baik seperti yang ditunjukkan daripada analisis UV-Vis bagi nanozarah pada panjang gelombang 437nm. Pengimejan SEM mendedahkan bahawa selepas penyingkiran templat PMMA daripada komposit Si-Alloy(Au-Ag)-PMMA, struktur songsang yang mempunyai struktur rangka lubang dihasilkan. Prestasi komposit Si-aloi(Au-Ag) songsang telah diuji melalui sel suria sensitif pewarna (DSSC) yang menunjukkan penguatan dalam bacaan voltan.

Kata kunci: struktur nano, fotonik, metalo-dielektrik, zarah nano aloi, opal songsang,

Introduction

Nobel laureate Richard Smalley once pointed out that energy and environmental problems will be the hardest challenges mankind will face in the next 50 years [1]. Solar photovoltaic (PV) technology gained traction as a popular renewable energy source due to its cost effectiveness, easy fabrication, and environmental friendliness [2]. In particular, solar cell devices, which harness sunlight and convert it into usable energy and electricity, became the focal interest of the photovoltaic industries that are ever-expanding due to the increasing prices of fossil fuel and to accelerate the push towards sustainable energy options [3]. Many endeavours had been made in researching and developing thin film materials that are capable of reducing costs of mass producing efficient solar strategies and mechanically flexible devices [4, 5]. Silicon is a prevalent material in solar cells, provided it yields strong low-light performances and is non-toxic [6, 7]. However, a shortcoming of the current silicon thin-film solar cells is the insufficient absorption of the near-bandgap light. The limitation could possibly be overcome by efficient light trapping which points towards the expansion of different light trapping geometries, one of which is the photonic crystal [8-10].

A photonic crystal is a periodic optical nanomaterial that manipulates the movement of the light (photons) directed by their lattice structure [11]. Photonic crystals have different dielectric constants and these materials cause a photonic band gap (PBG) that allows precise control over the flow of light [12]. This unique property has been applied in various advance technological devices such as sensors, photovoltaic and solar concentrators [13-16].

PMMA is used as the crystal template because higher yield of monodispersed particles can be produced [17]. PMMA will be synthesised through free-emulsifier emulsion polymerisation in water. This method is much safer for environment compared to methods that utilise toxic solvents such as toluene, dimethylformamide and dimethyl sulfoxide as medium of reaction. The removal of PMMA template results in inverse opal capable of achieving a complete band gap.

"Bottom up" method is used in the fabrication of film. This simple step reinforces the quality of long range ordered structures with greater strength. "Bottom up" co-crystallisation method is used rather than "top down" as the "top down" approach is complex, involves multisteps and costly procedures [18–20].

Materials and Methods Synthesis of PMMA colloidal nanoparticle

PMMA was synthesised through free-emulsifier emulsion polymerisation reaction with potassium persulphate as initiator, methyl methacrylate monomer, and deionised water as dispersion medium under nitrogen condition at 90 °C. The reaction was kept

stirring at speed of 350 rpm. Deionised water of 64 ml was bubbled with nitrogen gas and heated for 15 minutes at 90 °C. MMA monomer was added and kept stirring for 30 minutes. Lastly, potassium persulphate was added, with the solution kept stirring for another 40 minutes until polymerisation reaction was completed. The milky colloidal was centrifuged and washed for 6 times.

Synthesis of hydrolysed TEOS

Hydrolysed TEOS was prepared utilising the sol-gel method. Tetraethylorthosilicate (TEOS) of 1 ml, 8 ml of ethanol, and 1 ml of HCL were mixed together and stirred at speed of 350 rpm for 1 hour.

Synthesis of alloy(Au-Ag) nanoparticles

Deionised water of 78 ml was heated at $100 \, ^{\circ}C$. 1 ml of $0.05M \, HAuCl_4$, 1 ml of $0.05M \, AgNO_3$ and 8 ml of 0.1M sodium citrate were added and stirred for 15 minutes at $100 \, ^{\circ}C$.

Fabrication of inverted silica alloy(Au-Ag) film

Silica, alloy(Au-Ag), and PMMA film were prepared by utilising vertical deposition of the self-assembly method. A clean glass substrate was placed in the mixture of PMMA+TEOS+Alloy(Au-Ag) with a volume ratio of $50\mu l:5\mu l:40\mu l.$ Then, the mixture was placed in the oven for 3 days at 60 °C. Inverted silica and alloy(Au-Ag) were prepared by soaking the film in acetone and heated on hot plate at 300 °C to remove the PMMA template.

Results and Discussion

Characterisation of PMMA

The synthesised PMMA colloidal nanoparticles were investigated by using Fourier-transform infrared spectroscopy (FTIR). The FTIR spectra (Figure 1), of the synthesised PMMA was compared to MMA to gauge the complete polymerisation reaction of MMA to form PMMA. As shown in Table 1, there is a distinct difference in presence of C=C functional group between MMA and PMMA.

Table 1. Comparison of functional group of MMA and PMMA

Functional Group	Absorbance of MMA(cm ⁻¹)	Absorbance of PMMA(cm ⁻¹)
	H_2C CH_3 CH_3	CH ₃
О-Н	3437.68	3445.11
Sp ³ CH	2969.64-2857.88	2996.14-2843.33
C=O	1748.47	1731.91
C=C	1639.83	-
CH ₃	1329.97	1449.45 & 1388.57
C-O	1169.36	1242.77

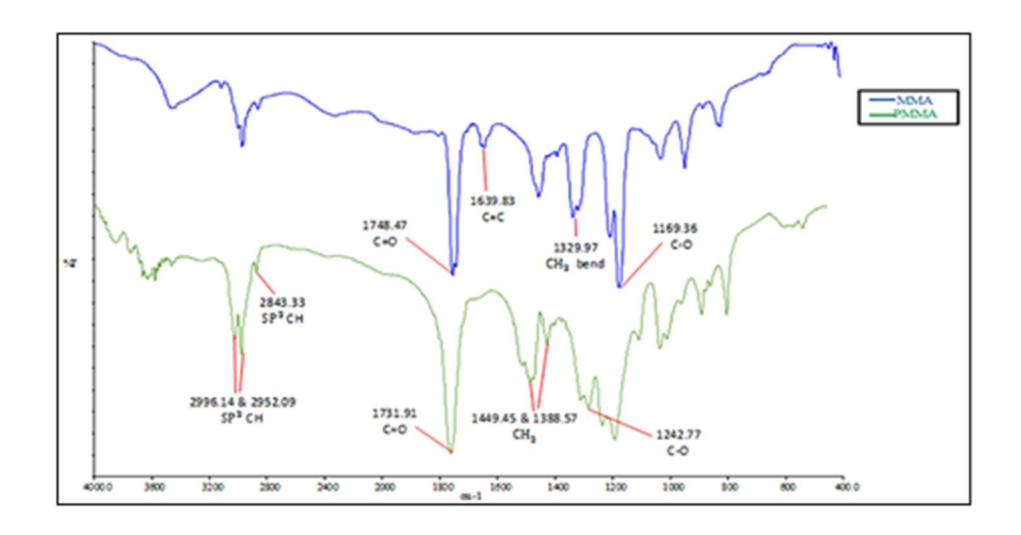


Figure 1. FTIR of methyl methacrylate(MMA) and poly(methyl methacrylate)

From the IR spectra obtained, the synthesised PMMA nanoparticles were concluded to be successful due to the absence of C=C peak at 1639.83 cm⁻¹ which would be present should there be incomplete polymerisation leaving residual MMA.

Structural elucidation of the synthesised PMMA was

determined by using X-ray diffraction (XRD). Figure 2 shows the XRD diffractogram of synthesised PMMA. PMMA powder was analysed in the range from 0 to 80 of 2θ at a scan speed of 2° /min. Bragg's angle was observed at $2\theta = 13.75^{\circ}$. Based on the XRD diffractogram, PMMA had a broad peak that suggested a complete amorphous, non-crystalline trait in nature.

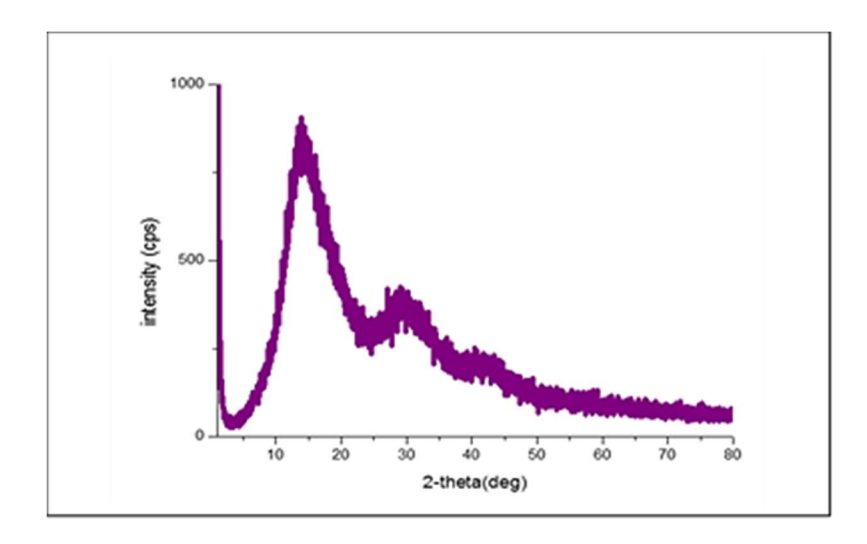


Figure 2. X-ray diffraction of synthesised PMMA

Thermogravimetric analysis (TGA) was used to further probe the purity and composition of the synthesised PMMA. Figure 3 shows the TGA curve, whereby the decomposition of PMMA and mass loss occurred in three stages.

According to Gałka et al. [21], thermal degradation of PMMA involved three stages; the first stage happened due to depolymerisation process that initiated involving head-to-head linkages, second stage involving unsaturated vinyl ends, and the last stage involving

chain scissions. For the synthesised PMMA, first stage of decomposition of PMMA occurred at 264 °C due to the loss of water and weak head-to-head bonds become decomposed. Second stage happened at 339 °C due to the radical transfer to unsaturated chain, which led to the decomposition of unsaturated chain-ends. Last stage of decomposition of PMMA occurred at 422 °C due to the

random scission of polymer chains. These results conformed to established thermogravimetric analysis of PMMA thermal stability, suggesting that the success in PMMA synthesis via the method of free-emulsifier emulsion polymerisation reaction, which was the 'greener' option for fabrication.

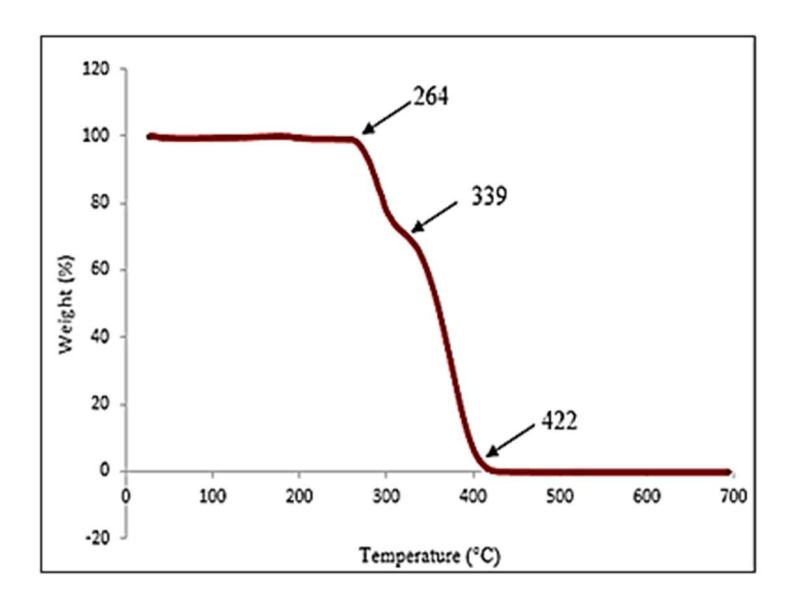


Figure 3. TGA graph of the synthesised PMMA

The surface morphology of PMMA was characterised by using scanning electron microscopic (SEM). Figure 4 shows that the PMMA produced were homogeneous sphere-shaped particles with average size of 495 nm. The homogeneous sphere shape of PMMA was obtained due to the stable control temperature throughout the experiment. Centrifugation also aided in separating

PMMA particles based on density and eliminated the small particles of PMMA. The SEM images also shows the formation of well-ordered arrangement of the nanosized particles. The PMMA particles were not aggregated and had good monodispersity, which was fundamental for yielding high quality photonic crystals.

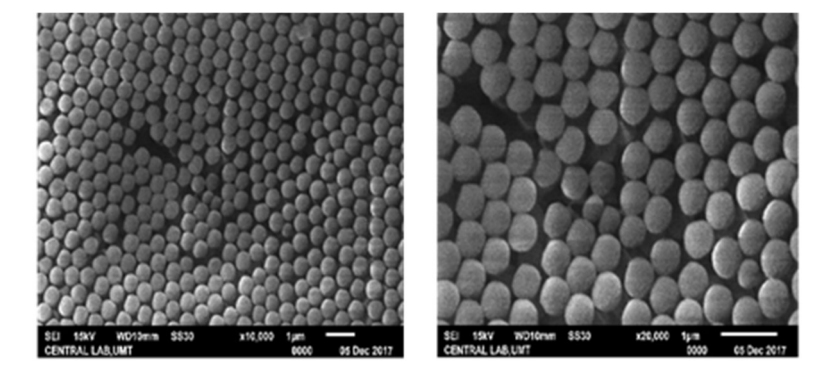


Figure 4. Scanning electron microscopic characterization of synthesised PMMA at 20000x (left) and 10000x (right)

Characterisation of hydrolysed TEOS

Hydrolysed TEOS was prepared utilising sol-gel polymerisation and the functional groups of the TEOS molecule were determined by Fourier-transform infrared spectroscopy (FTIR). The functional groups in the FTIR spectra of the hydrolysed TEOS (Figure 5), is translated into Table 2.

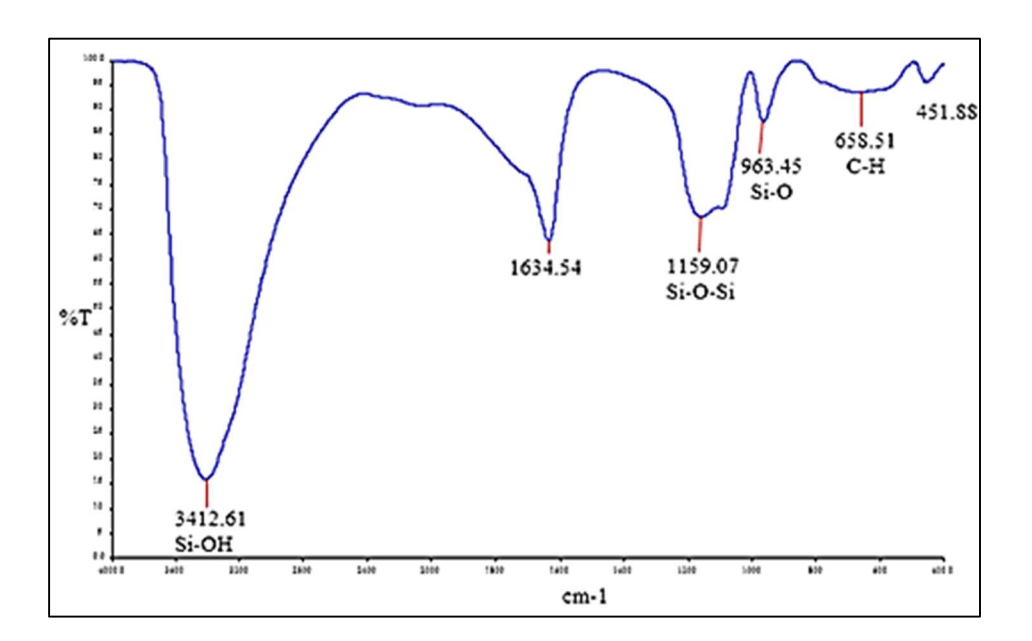


Figure 5. FTIR of hydrolysed TEOS

Table 2. Functional groups of hydrolysed TEOS

Molecular Structure of TEOS

where R is an alkyl chain

•		
Vibrational mode	Hydrolysed TEOS (cm ⁻¹⁾	
Si-OH	3412.61	
Si-O-Si	1159.07	
Si-O	963.45	
С-Н	658.51	

A strong peak can be seen at 3412.61 cm⁻¹ due to the stretching of Si-OH bond. Peak at 1159.07 cm⁻¹ indicated the formation of Si-O-Si bond. A weak peak appeared at 963.45 cm⁻¹ due to the Si-O bond. Lastly, C-

H peak appeared at 658.51 cm⁻¹. This indicated the successful synthesis of hydrolysed TEOS to be used as the cementing component. The sol-gel polymerisation method involved hydrolysis and condensation

processes. First, TEOS underwent catalytic hydrolysis in the presence of HCL and water. Ethanol was added as a homogenising agent between water and TEOS, which were immiscible, and HCL was added to expediate the hydrolysis process. The condensation reaction took place under acidic condition. The Si became more electrophilic and susceptible to nucleophilic attack, forming a longer polymer network.

Characterisation of alloy(Au-Ag)

Au and Ag can strongly interact with sunlight. Silver is the commonly chosen metal nanoparticle due to its low cost and great absorption. However, silver is not the most stable. On the other hand, gold is much more stable in comparison. According to Al-Azawi et al. [22], the bimetallic nanoparticle (Au–Ag alloy nanoparticle) structure possessed a good stability, a greater ability to absorb light in a wider range of wavelength (broad LSPR peak). Also, capacity to tune the nanoparticle optical properties compared with that originating from individual nanoparticle. These; thus suggested a potential in increasing the effectiveness of a solar cell.

Absorption of alloy(Au-Ag) was determined by using ultra-violet visible spectroscopy. Typical absorption of Au is located at 521 nm, and Ag at 407 nm. Figure 6 shows a single absorption peak at 437 nm, which is the intermediate position between typical absorption of Au and Ag. This broad absorption band strongly indicated the formation of Au–Ag alloy NPs and not simply a mixture of Au and Ag NPs.

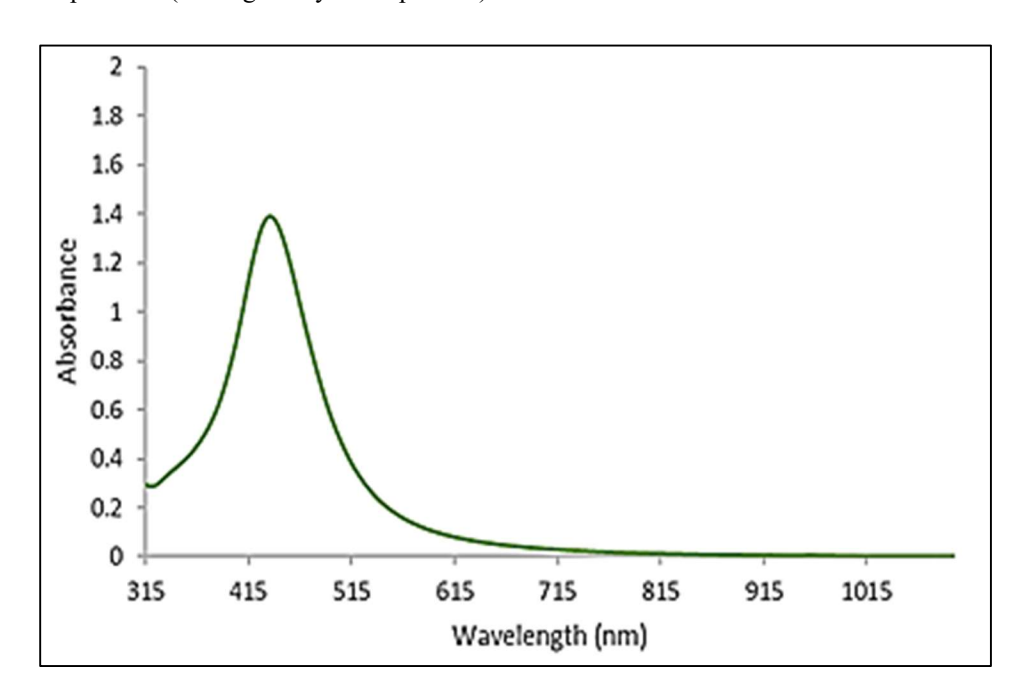


Figure 6. Ultraviolet-visible spectroscopy of alloy(Au-Ag)

Figure 7 shows the morphology of alloy(Au-Ag) characterised by SEM. SEM image revealed the properties of aggregation of alloy(Au-Ag) nanoparticle. Based on SEM image, alloy(Au-Ag) with volume ratio 1:3 had a uniform spherical shape. Au has a tendency to aggregate more than Ag due to its smaller size.

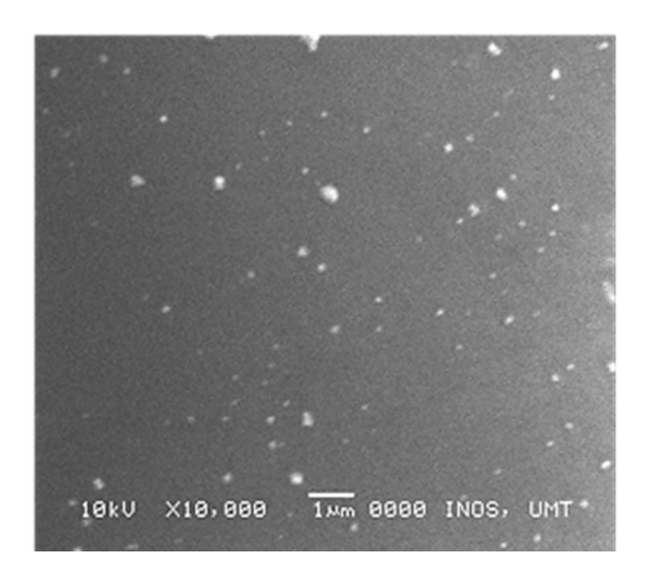


Figure 7. Morphology of alloy(Au-Ag).

Characterisation of inverted silica alloy(Au-Ag) film The surface morphology of silica-PMMA, inverted silica, PMMA-silica-Alloy(Au-Ag) and inverted silicaalloy(Au-Ag) had been characterised by using scanning electron microscope (SEM) as shown in Figure 8.

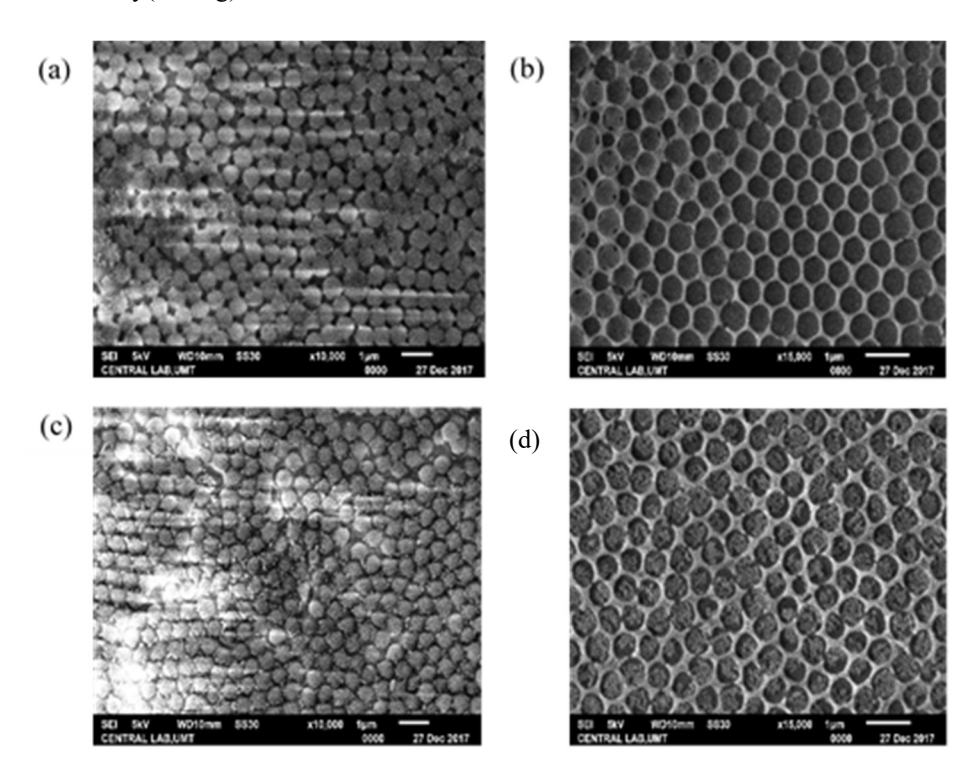


Figure 8. SEM image of silica-PMMA morphology (a), inverted silica morphology (b), silica-PMMA-alloy(Au-Ag) morphology (c), and inverted silica-alloy(Au-Ag) morphology (d)

The morphology of silica-PMMA (a) was sphere-shaped with homogenous structure of the same size. The addition of hydrolysed TEOS held the PMMA structure together and prevented cracking in the film. The structure was packed closely with almost consistentlysized spaces in between. The morphology of the inverted silica (b) showed a skeleton structure of silica after the removal of PMMA. The 'holes' were almost uniform in size and arrangement. With the addition of alloy(Au-Ag) into the solution of silica-PMMA, morphology of PMMA-silica-alloy(Au-Ag) (c) appeared to also possess spherical shape with homogenous structure of the same size, including the presence of alloy(Au-Ag) scattered around the PMMA. The morphology of the inverted silica-alloy(Au-Ag) (d) too had a skeleton structure, similar to the inverted silica (b). However, the inverted silica-alloy(Au-Ag) (d) had a 'grainy' appearance from the successful embedding of the alloy(Au-Ag) within the inverted silica structure. Precise control must be applied to obtain a completely inverted structure by tuning the volume ratio of PMMA suspension, alloy nanoparticles solution and TEOS solution during fabrication. The average diameter of the

hole was observed to shrink after the removal of PMMA spheres. However, no silica backbone cracking was observed. This proved that the suitability of hydrolysed silica or TEOS as cementing agent for crack-free inverted structure. This inverted structure with the plasmonic properties of the alloy(Au-Ag) has potential in increasing the light trapping capabilities, particularly in increasing the effectiveness of a solar cell.

Performance of inverted structure towards dye sensitive solar cell (DSSC)

Inverted Si-alloy(Au-Ag) substrate with spherical holes structure contained voids that had the potential in fully trapping light within a solar cell for photovoltaic applications. The performance of inverted Si-alloy(Au-Ag) substrate in DSSC was tested by utilising a multimeter. Figure 9 illustrates the multimeter setup. It was found that the voltage reading of the multimeter increased by 0.4V when the inverted silica-alloy(Au-Ag) was applied. This showed that the inverted structure, possessing plasmonic properties of alloy(Au-Ag), had successfully trapped light and the increased the voltage of the multimeter.

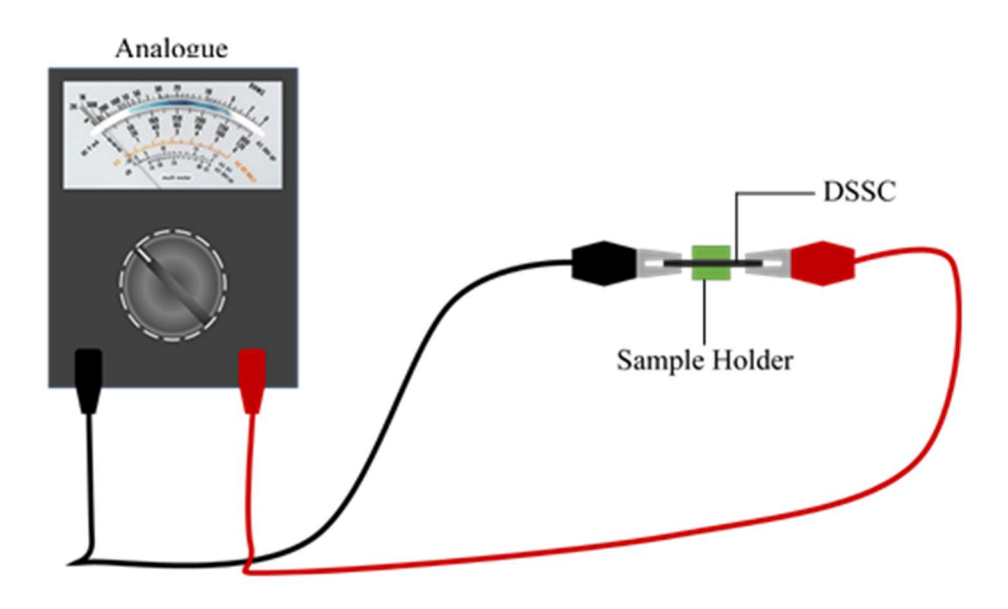


Figure 9. Simplified illustration of the multimeter setup

Conclusion

Photonic crystals or photonic band gap materials have harnessed global interest for the past decades due to the special periodic structure capable of modulating the propagation of electromagnetic waves [23, 24]. Presently, more attention is turned towards adapting inverted opal photonic crystals in light trapping and solar energy harvesting, allowing improvements in the photo-collection efficiency in dye desensitised solar cell (DSSC) and silicon solar cell through enhanced electron transport [13, 24].

In this work, the researchers presented the fabrication and structural, and optical characterisations of inverted Si-alloy(Au-Ag) composite photonic crystal via cocrystallisation method involving tetraethyl orthosilicate (TEOS) solution, poly(methyl methacrylate) (PMMA) spheres, and alloy of gold and silver nanoparticles. Polymer PMMA was synthesised via free-emulsifier emulsion polymerisation and used as template. Freeemulsifier emulsion polymerisation is an environmentfriendly method of synthesising PMMA because of the absence of harmful surfactants that negatively impact the environment, particularly wastewater pollution. The reaction utilised water as dispersion medium instead of toxic solvents. The complete polymerisation of PMMA from MMA via this technique was confirmed via the absence of C=C peak at 1639.83 cm⁻¹ in the FTIR spectra and further characterised via XRD diffraction analysis, thermogravimetric analysis, which aligned with the established pattern of PMMA TGA curve. Also, SEM analysis that revealed homogeneous sphereshaped PMMA nanospheres of 495 nm in average size and good monodispersity. TEOS was successfully prepared via sol-gel polymerisation consisting of hydrolysis and condensation reaction. The initial reaction began with the use of an alkoxysilane in ethanol and resulted in a solution of siloxane polymer suitable to be used to produce a crack-free inverted structure. The FTIR spectra of TEOS collated with the molecular structure of hydrolysed TEOS to be used as cementing component. TEOS used in this research is a cheaper and non-toxic alternative to other silica precursors. Gold and silver nanoparticles were alloyed and characterised through UV-vis spectroscopy and SEM analysis. The synthesis of alloy(Au-Ag) was deemed successful as the

absorption spectra of the produced alloy nanoparticles was absent of single Au and Ag absorbance peaks, indicating the absence of single Au and Ag species in the solution. Inverted silica alloy(Au-Ag) film was successfully synthesised via co-crystallisation method by implementing 'bottom-up' vertical deposition fabrication method. At each stage of the fabrication process, SEM analysis was conducted. The SEM imaging of silica-PMMA, inverted silica, silica-PMMAalloy(Au-Ag), and inverted silica-alloy(Au-Ag) compared the 3D nanostructures pre-PMMA removal and post-removal through calcination process, and the absence and presence of the alloy(Au-Ag). The inverted silica-alloy(Au-Ag) film fabricated possessed consistent skeleton hole structure of rough-textured grainy surface appearance, notably ideal for light manipulating functions [25, 26].

In this paper, the researchers also investigated briefly the effect of silica-alloy(Au-Ag) substrate towards DSSC, as it is one of the most common purposes of photonic crystals in solar technology. The two are almost synonymously mentioned in any search. The inverted structure of silica-alloy(Au-Ag) had proven to trap light within a solar cell, consequently increasing its effectiveness. This is due to the skeletal structure of the substrate combined with the plasmonic properties of alloy(Au-Ag) of which increased the multimeter reading by 0.4V once applied.

The systematic light trapping properties of inverted silica-alloy(Au-Ag) nanostructure provide much room for future work in exploring further applications of the material synthesised in this work. Surface-enhanced Raman spectroscopy (SERS) is an excellent vibrational analytical technique for probing minute molecules bound in proximity to plasmonic surfaces [27,28]. The material synthesised in this study allowed for effective light trapping and photon density state, combining with the alloy nanoparticles of Ag that produced impressive SERS signal intensities, and Au that is highly resistant to oxidation [29]. Aside from that, the procedures in synthesising these substantially homogenous inverse silica-alloy(Au-Ag) by using PMMA and environmentfriendly surfactant-free dispersion medium and linking agent makes mass producing this material an easier,

cheaper, a 'greener' sustainable approach to SERS substrate. Inverse silica-alloy(Au-Ag) requires a short fabrication time and could be integrated into plasmonic biosensors and point-of-care devices in the studying and monitoring of disease progression. Moreover, the composite could be easily modified or coated to be relatively safe and biocompatible for further study in in vivo applications [30,31]. Optical microchips could significantly minimise the power consumption of computers and permits exponentially faster data processing speed. With some fine-tuning, the photonic band gap of 3D silica-alloy(Au-Ag) photonic crystal allows for not just the simple trapping of light but also guiding light beyond the traditional method that is rooted in total internal reflection, such as optical fibres Incorporation of silica-alloy(Au-Ag) optoelectronics could be made possible in offering important advantages over 2D electronic chips and expand the class of optical telecommunications in a variety of fields, including engineering and medicine in future studies [33].

Acknowledgement

We would like to express our acknowledgement to the Ministry of Education of Malaysia for Fundamental Research Grant Scheme (FRGS) 59630 (FRGS/1/2020/STG05/UMT/02/4) and Universiti Malaysia Terengganu for research supports and facilities.

References

- Shakeel Ahmad, M., Pandey, A. K. and Abd Rahim, N. (2017). Advancements in the development of TiO₂ photoanodes and its fabrication methods for dye sensitized solar cell (DSSC) applications. A review. Renewable and Sustainable Energy Reviews, 77: 89-108.
- Wang, Z., Tang, Y., Li, M., Zhu, Y., Li, M., Bai, L., Luoshan, M., Lei, W. and Zhao, X. (2017). Plasmonic enhancement of the performance of dyesensitized solar cells by incorporating TiO₂ nanotubes decorated with Au nanoparticles. *Journal of Alloys and Compounds*, C (714): 89-95.
- 3. Aberle, A. G. (2009). Thin-film solar cells. *Thin Solid Films*, 517(17): 4706-4710.
- 4. Andreani, L. C., Bozzola, A., Kowalczewski, P. and

- Liscidini, M. (2015). Photonic light trapping and electrical transport in thin-film silicon solar cells. *Solar Energy Materials and Solar Cells*, 135: 78-92.
- 5. Zanotto, S., Liscidini, M. and Claudio Andreani, L. (2010). Light trapping regimes in thin-film silicon solar cells with a photonic pattern. *Optics Express*, 18(5): 4260-4272.
- 6. Werner, J., Weng, C.-H., Walter, A., Fesquet, L., Seif, J. P., De Wolf, S., Niesen, B. and Ballif, C. (2016). Efficient monolithic perovskite/silicon tandem solar cell with cell area >1 cm². *The Journal of Physical Chemistry Letters*, 7(1): 161-166.
- Eisenlohr, J. (2017). Light trapping in highefficiency crystalline silicon solar cells. Doctoral dissertation, University of Konstanz, Germany.
- 8. Cao, D. H., Stoumpos, C. C., Farha, O. K., Hupp, J. T. and Kanatzidis, M. G. (2015). 2D homologous perovskites as light-absorbing materials for solar cell applications. *Journal of the American Chemical Society*, 137(24): 7843-7850.
- Ouanoughi, A., Hocini, A. and Khedrouche, D. (2016). Enhanced absorption of solar cell made of photonic crystal by geometrical design. *Frontiers of Optoelectronics*, 9(1): 93-98.
- Li, Y., Chen, Y., Ouyang, Z. and Lennon, A. (2015). Angular matrix framework for light trapping analysis of solar cells. *Optics Express*, 23(24): A1707-A1719.
- Kassim, S., Mcgrath, J. and Padmanabhan, S. (2015). Preparation and properties of silica inverse opal via self-assembly. *Applied Mechanics and Materials*, 699: 318-324.
- 12. Chen, W., Meng, Z., Xue, M. and Shea, K. (2016). Molecular imprinted photonic crystal for sensing of biomolecules. *Molecular Imprinting*, 4: 1-12.
- 13. Lonergan, A., McNulty, D. and O'Dwyer, C. (2018). Tetrahedral framework of inverse opal photonic crystals defines the optical response and photonic band gap. *Journal of Applied Physics*, 124(9): 095106.
- 14. Armstrong, E. and O'Dwyer, C. (2015). Artificial opal photonic crystals and inverse opal structures fundamentals and applications from optics to energy storage. *Journal of Materials Chemistry C*, 3(24): 6109-6143.

- Garín Escrivá, M., Hernández, D., Trifonov, T. and Alcubilla, R. (2014). Three-dimensional metallodielectric selective thermal emitters with hightemperature stability for thermophotovoltaic applications. Solar Energy Materials and Solar Cells, 134: 22-28.
- 16. Rout, D. and Vijaya, R. (2017). Role of stopband and localized surface plasmon resonance in raman scattering from metallo-dielectric photonic crystals. *Plasmonics*, 12(5): 1409-1416.
- 17. Kassim, S. (2014). Polymer and metallodielectric based photonic crystals. Doctoral thesis, University College Cork, Ireland.
- 18. Kassim, S., Mukhtar, N. A. and Tahrin, R. A. A. (2020). Synthesis and characterization of plasmonenhanced SERS substrate based on Au-Ag alloycoated, large-area photonic (methyl methacrylate+styrene) co-polymer. *Materials Science Forum*, 982: 14-19.
- Kassim, S., Padmanabhan, S. C. and Pemble, M. E. (2021). Bottom-up colloidal synthesis of PMMA@Au core-shell based metallodielectric photonic crystals as substrates for surface-enhanced Raman spectroscopy. *Applied Surface Science*, 569: 151014.
- Padmanabhan, S.C., Kassim, S. and Pemble, M. (2018). Colloidal co-crystallization: A new route for production of three-dimensional metallodielectric photonic crystals. *Asian Journal of Chemistry*, 30(7): 1613-1616.
- Gałka, P., Kowalonek, J. and Kaczmarek, H. (2014). Thermogravimetric analysis of thermal stability of poly(methyl methacrylate) films modified with photoinitiators. *Journal of Thermal Analysis and Calorimetry*, 115(2): 1387-1394.
- 22. Al-Azawi, M. A., Bidin, N., Bououdina, M. and Mohammad, S. M. (2016). Preparation of gold and gold–silver alloy nanoparticles for enhancement of plasmonic dye-sensitized solar cells performance. *Solar Energy*, 126: 93-104.
- 23. Marichy, C., Muller, N., Froufe-Pérez, L. S. and Scheffold, F. (2016). High-quality photonic crystals with a nearly complete band gap obtained by direct inversion of woodpile templates with titanium dioxide. *Scientific Reports*, 6(1): 21818.

- Shishkin, I. I., Rybin, M. V., Samusev, K. B., Golubev, V. G. and Limonov, M. F. (2014). Multiple Bragg diffraction in opal-based photonic crystals: Spectral and spatial dispersion. *Physical Review B*, 89(3): 035124.
- 25. Wang, Z. and Yu, B. (2018). Plasmonic control of refractive index without absorption in metallic photonic crystals doped with quantum dots. *Plasmonics*, 13(2): 567-574.
- Van Lare, C., Lenzmann, F., Verschuuren, M. A. and Polman, A. (2015). Dielectric scattering patterns for efficient light trapping in thin-film solar cells. *Nano Letters*, 15(8): 4846-4852.
- 27. Byrne, H. J., Baranska, M., Puppels, G. J., Stone, N., Wood, B., Gough, K. M., Lasch, P., Heraud, P., Sulé-Suso, J. and Sockalingum, G. D. (2015). Spectropathology for the next generation: Quo vadis? *Analyst*, 140(7): 2066-2073.
- Yang, S., Dai, X., Stogin, B. B. and Wong, T.-S. (2016). Ultrasensitive surface-enhanced Raman scattering detection in common fluids. *Proceedings of the National Academy of Sciences*, 113(2): 268-273.
- Shukla, R., Bansal, V., Chaudhary, M., Basu, A., Bhonde, R. R. and Sastry, M. (2005). Biocompatibility of gold nanoparticles and their endocytotic fate inside the cellular compartment: A microscopic overview. *Langmuir*, 21(23): 10644-10654.
- 30. Du, Z., Qi, Y., He, J., Zhong, D. and Zhou, M. (2021). Recent advances in applications of nanoparticles in SERS in vivo imaging. *WIREs Nanomedicine and Nanobiotechnology*, 13(2): e1672.
- 31. Samanta, A., Maiti, K. K., Soh, K.-S., Liao, X., Vendrell, M., Dinish, U. S., Yun, S.-W., Bhuvaneswari, R., Kim, H., Rautela, S., Chung, J., Olivo, M. and Chang, Y.-T. (2011). Ultrasensitive Near-Infrared Raman Reporters for SERS-Based In Vivo Cancer Detection. *Angewandte Chemie*, 123(27): 6213-6216.
- 32. Götz, S. and Karst, U. (2007). Recent developments in optical detection methods for microchip separations. *Analytical and Bioanalytical Chemistry*, 387(1): 183-192.

33. Kumar, V. V. R. K., George, A. K., Knight, J. C. and Russell, P. S. J. (2003). Tellurite photonic crystal fiber. *Optics Express*, 11(20): 2641-2645.